Med, Volume *3*

Supplemental information

Discovery and intranasal administration of a SARS-CoV-2 broadly acting neutralizing antibody with activity against multiple Omicron subvariants

J. Andrew Duty, Thomas Kraus, Heyue Zhou, Yanliang Zhang, Namir Shaabani, Soner Yildiz, Na Du, Alok Singh, Lisa Miorin, Donghui Li, Karen Stegman, Sabrina Ophir, Xia Cao, Kristina Atanasoff, Reyna Lim, Ignacio Mena, Nicole M. Bouvier, Shreyas Kowdle, Juan Manuel Carreño, Laura Rivero-Nava, Ariel Raskin, Elena Moreno, Sachi Johnson, Raveen Rathnasinghe, Chin I. Pai, Thomas Kehrer, Elizabeth Paz Cabral, Sonia Jangra, Laura Healy, Gagandeep Singh, Prajakta Warang, Viviana Simon, Emilia Mia Sordillo, Harm van Bakel, Yonghong Liu, Weina Sun, Lisa Kerwin, John Teijaro, Michael Schotsaert, Florian Krammer, Damien Bresson, Adolfo García-Sastre, Yanwen Fu, Benhur Lee, Colin Powers, Thomas Moran, Henry Ji, Domenico Tortorella, and Robert Allen

Supplemental Figure 1.

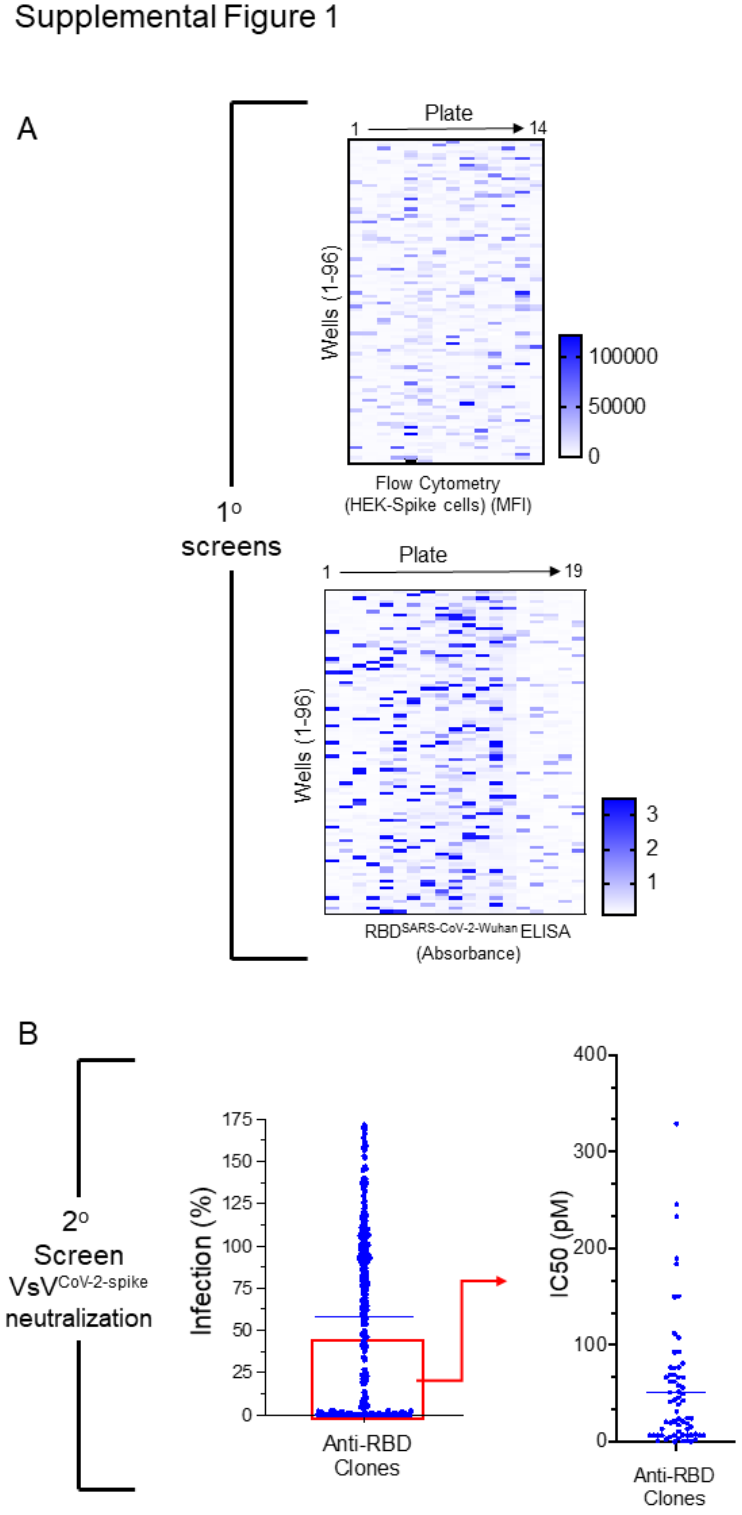

Supplemental Figure 1: Discovery of SARS-CoV-2 Neutralizing Antibodies from Mouse 3. Related to Figure 1.

(A) Primary screens based on the anti-RBD hybridoma clones from mouse 3(M-3) were performed by flow-cytometry using Expi293F cells transfected with SARS-CoV-2 Wuhan strain spike protein and RBD ELISA. Upon flow cytometry analysis, the mean fluorescence intensity (MFI) was determined for each clone. The RBD-ELISA represents binding of the clones to RBD as measured by absorbance. Both the flow cytometry and ELISA data are represented as heat maps. (B) The secondary assays for the binding clones were a VSV-spike^{CoV-2} neutralization assay followed by the determination of IC50 (pM) for clones with > 50% neutralization activity.

Supplemental Figure 2.

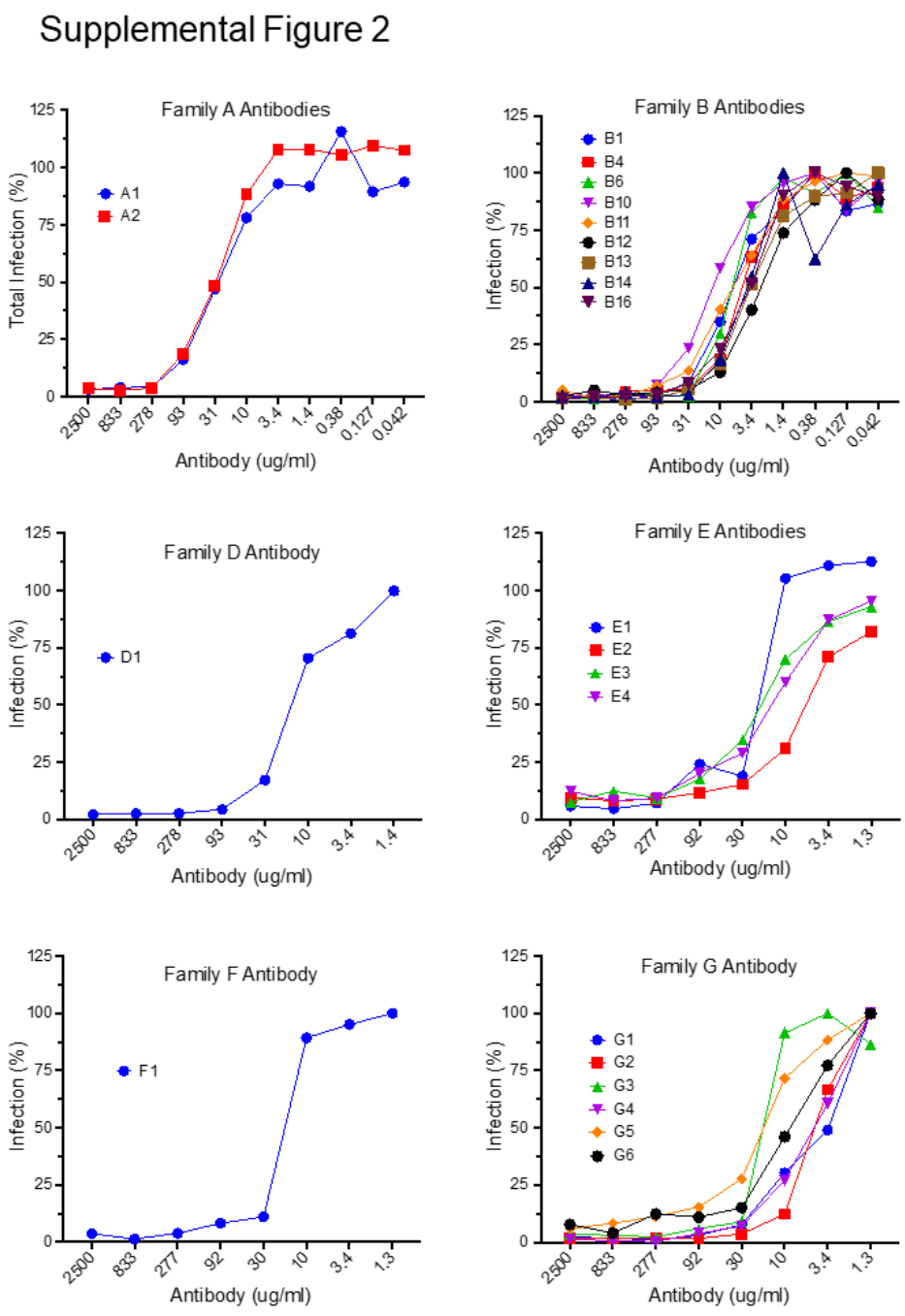

Supplemental Figure 2: Analysis of neutralization activity of anti-SARS-CoV-2 clones.

Related to Figure 1.

HEK-293 expressing hACE2/TMPRSS2 cells (10,000 cells/well of 96 well plate) were infected with VSV-spike^{CoV-2} pre-incubated with increasing concentrations of individual antibodies from the different antibody Families. At 24 hours post-infection, the cells were detached using non-enzymatic dissociation reagent and resuspended in cold FACS buffer and analyzed by flow cytometry (Intellicyte Corp., Albuquerque, NM) for GFP fluorescence intensity. The % of GFP positive cells was identified from each sample and % of GFP positive cells from mock-treated virus was used as 100% infection. The data was normalized to 100% infection and the IC50 was determined by GraphPad Prism using [Inhibitor] vs. normalized response-variable slope.

Supplemental Figure 3.

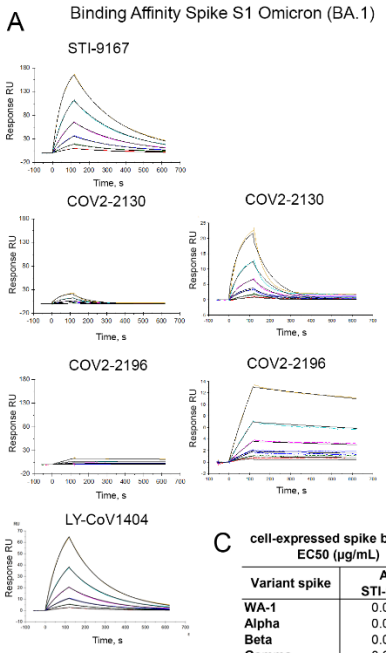

C

cell-expressed spike binding EC50 (μg/mL)

Variant spike	Ab STI-9167
WA-1	0.025
Alpha	0.019
Beta	0.015
Gamma	0.014
Delta Plus	0.043
Lambda	0.0089

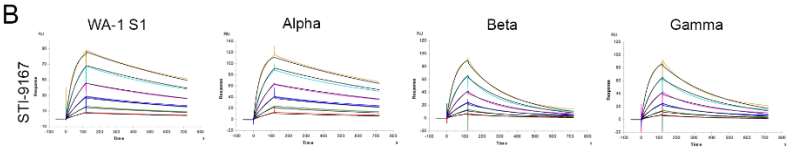

Variant RBD	ka (1/Ms) Ab STI-9167	kd (1/s) Ab STI-9167	KD (M) Ab STI-9167	Rmax (RU) Ab STI-9167	Chi² (RU²) Ab STI-9167
WA-1	2.27 ± 0.2 E+05	1.40 ± 0.03 E-03	6.20 ± 0.44 E-09	97.2 ± 4.3	1.19 ± 0.30
Alpha	2.65 ± 0.2 E+05	1.32 ± 0.03 E-03	5.04 ± 0.04 E-09	105.4 ± 6.5	1.56 ± 0.24
Beta	2.12 ± 0.2 E+05	6.84 ± 0.12 E-03	3.24 ± 0.26 E-08	108.3 ± 6.6	0.14 ± 0.02
Gamma	2.57 ± 0.2 E+05	5.23 ± 0.05 E-03	2.04 ± 0.16 E-08	104.9 ± 5.6	0.53 ± 0.04

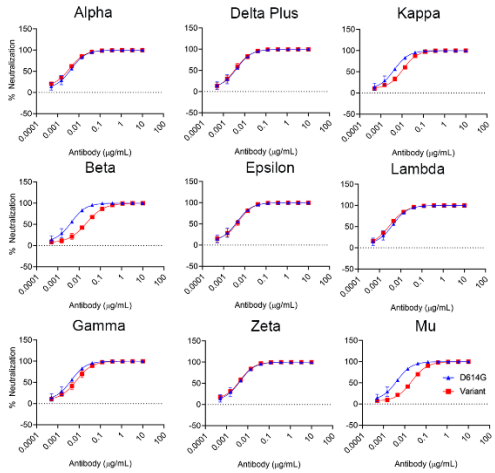

Pseudotype neutralization IC50 (μg/mL)

Virus	Ab STI-9167
Alpha	0.0029
Beta	0.0195
Gamma	0.0063
Delta Plus	0.0033
Epsilon	0.0040
Zeta	0.0034
Kappa	0.0090
Lambda	0.0027
Mu	0.0186

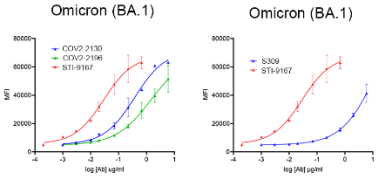

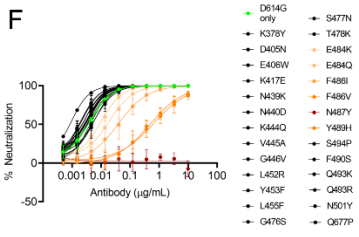

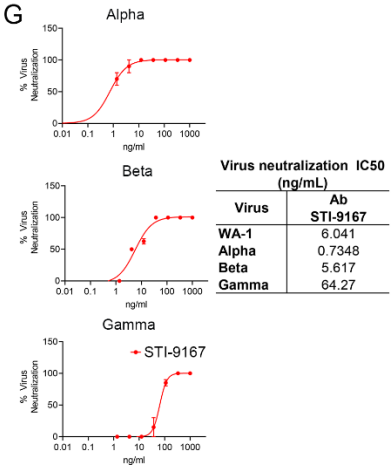

Virus neutralization IC50 (ng/mL)

Virus	Ab STI-9167
WA-1	6.041
Alpha	0.7348
Beta	5.617
Gamma	64.27

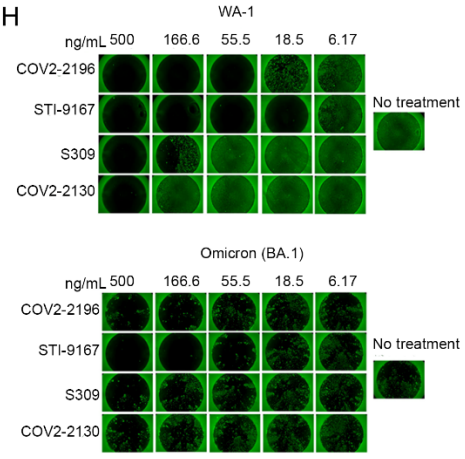

Supplemental Figure 3. Binding and neutralization of candidate antibody to VoCs.

Related to Figure 2. (A) SPR binding affinity graphs of antibodies STI-9167, COV2-2130, COV2-2196, and S309. (B) Affinity measurements of STI-9167 against the Spike S1 binding domain from SARS-CoV-2 isolates and VOCs: USA/WA-1/2020(WA-1) isolate, Alpha, Beta, and Gamma. The antibody affinities were measured using SPR on a BIAcore T200 instrument using a 1:1 binding model. Graphs are representative of triplicate data and table data presented as mean ± SD. (C) Spike protein derived from Alpha, Beta, Gamma, Delta Plus, and Lambda SARS-CoV-2 isolates were independently expressed on the surface of HEK 293 cells. Serially-diluted STI-9167 was assayed for spike protein binding to the transfected spike cells by flow cytometry. To quantify antibody binding, mean fluorescent intensity was measured for each dilution tested and the EC_{50} value was calculated for each nAb. (D) Spike-pseudotyped VSV neutralization. Antibody neutralization curves of the pseudotyped VSVs spike variants (Material and Methods) is representative of three independent experiments, with error bars representing one standard deviation. IC50 values for each pseudotype/antibody combination are indicated . (D) PRNT assay using STI-9167 withSARS-CoV-2 variants were performed (Material and Methods). (E) Omicron spike protein was expressed on HEK 293 cells and binding of selected neutralizing antibodies was measured by MFI using flow cytometry. (F) Pseudotyped VSVs were generated from vectors of SARS-CoV-2 Spike Wuhan strain carrying the D614G substitution with an additional amino acid substitution in the RBD. Pseudotype VSV-spike neutralization assays were performed using STI-9167 (Materials and Methods, duplicate experimental runs in technical triplicate repeats) to determine the potential structural constraints of STI-9167 neutralization. Curves were generated using non-linear regression with constraints of 100 (top) and 0 (baseline). Parental Spike D614G only is color coded in green. Additional substitutions that led to IC50 values >2 fold higher than

D614G are colored, while all other substitutions are in black. (G) PRNT assay using STI-9167 withSARS-CoV-2 variants were performed to determine IC50 values (μg/ml) (Material and Methods). (H) PRNT assay using STI-9167 and various neutralizing antibodies with SARS-CoV-2 WA-1 or Omicron were performed (Material and Methods) on Vero-ACE2-expressing cells.

Supplemental Figure 4.

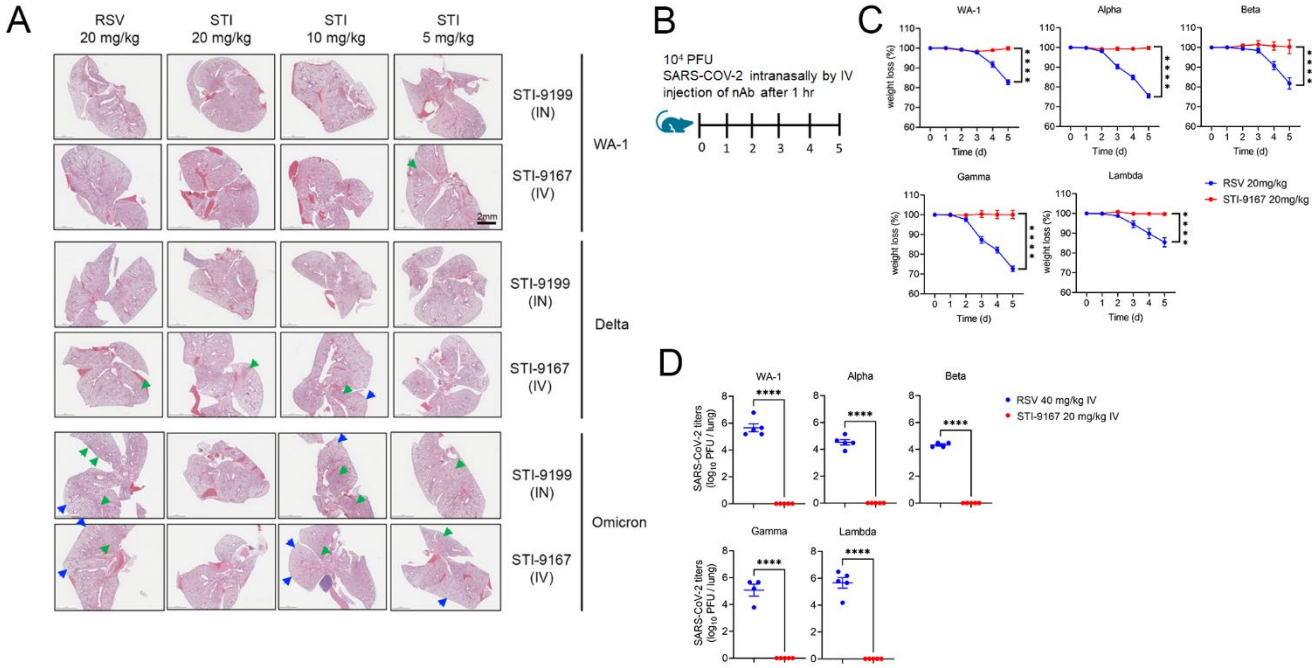

Supplemental Figure 4. Efficacy of Intranasal (IN) delivery of STI-9167 neutralizing antibody in the K18-hACE2 murine model of COVID-19 VOCs.

Related to Figure 4. (A) H&E staining of lung tissue was performed on mice infected with WA-1, Delta and Omicron and treated with indicated concentrations of antibody, either administered IV or IN. Representative images are shown (scale bar, 2 mm). Generally, areas of dense consolidation in H&E sections correspond to virus-infected areas in IHC sections (green arrowheads), while the

aerated/non-consolidated lung parenchyma corresponds to an absence of virus staining in IHC (blue arrowheads). (B) A schematic of experimental model, K18-hACE2 transgenic mice were infected with 10000 PFU of indicated variants of SARS-CoV-2 treated with indicated concentration of nAb (STI-9167) intravenously 1 hour post infection. (C) Body weight change of mice was measured daily (n = 5). (D) SARS-CoV-2 viral titers were measured in lung day 5 post infection (n = 5). P****<0.0001 values were determined using a two-way ANOVA (B) and unpaired t test (D).

Supplemental Table 1. SARS-CoV-2 Variants and Mutations. Related to Methods Section.

Variant	Mutations (and mutations in RBD from 333 to 526)
B1.1.7/Alpha variant	deletion of 69-70, deletion of Y144, N501Y, A570D, D614G, P681H, T716I, S982A, D1118H
B1.351/Beta variant	L18F, D80A, D215G, deletion of 242-244, R246I, K417N, E484K, N501Y, D614G, A701V
P.1/Gamma variant	L18F, T20N, P26S, D138Y, R190S, K417T, E484K, N501Y, H655Y, T1027I
B.1.526/Iota variant	L5F, T95I, D253G, E484K, D614G, A701V
B.1.427/B.1.429/Epsilon variant	S13I, W152C, L452R
B.1.427/B.1.429/Epsilon variant	T478K, D614G
B.1.617.1/Kappa variant	T95I, G142D, E154K, L452R, E484Q, D614G, P681R, Q1071H, H1101D
B.1.617.2/Delta variant	T19R, T95I, G142D, deletion of 157-158, A222V, L452R, T478K, D614G, P681R, D950N
B.1.1.529/Omicron (BA.1) variant	A67V, del69-70, T95I, G142D, del143-145, N211D, del212, G339D, S371L, S373P, S375F, K417N, N440K, G446S, S477N, T478K, E484A, Q493R, G496S, Q498R, N501Y, Y505H, T457K, D614G, H665Y, N679K, P681H, N764K, D796Y, N856K, Q954H, N969K, L981F
B.1.1.529/Omicron + R346K (BA.1.1) variant	A67V, del69-70, T95I, G142D, del143-145, N211D, del212, G339D, R346K, S371L, S373P, S375F, K417N, N440K, G446S, S477N, T478K, E484A, Q493R, G496S, Q498R, N501Y, Y505H, T457K, D614G, H665Y, N679K, P681H, N764K, D796Y, N856K, Q954H, N969K, L981F
BA.2	T19I, L24S, del25-27, G142D, V213G, G339D, S371F, S373P, S375F, T376A, D405N, R408S, K417N, N440K, S477N, T478K, E484A, Q493R, Q498R, N501Y, Y505H, H655Y, N679K, P681H, N764K, D796Y, Q954H, N969K